New Schiff Base and Its Zn^{2+} Metallopolymer: Synthesis, Characterization and Solid-State Conductivity

Esmaeili, Alireza; Grivani, Gholamhossein*+

School of Chemistry, Damghan University, Damghan, I.R. IRAN

ABSTRACT: *The N, N'-bis-pyridine-4-ylmethylene-1,2-diamine (Pyen) was prepared by a reaction of ethylene diamine and 4- pyridine carbaldehyde. The DA was synthesized by a reaction of 4- chloromethyl salicylaldehyde and Pyen. The new ionic Schiff base polymer ligand (L) was synthesized by a reaction of DA and ethylene diamine in methanol at refluxed conditions. The ionic Zn^{2+}mettallo Schiff base polymer was synthesized by reaction of L and $ZnCl_2$ in methanol at refluxed conditions. The synthesized compounds were characterized by various analytical and spectral methods. The chemical composition and functional group identification of the synthesized compounds were confirmed by CHN analysis, FT-IR, ^{1}H-NMR spectroscopy, and mass spectrometry. The molecular weight of the L and ZnL was determined by size exclusion chromatography with the results of the M_w= 6441.4 and 14212 for L and ZnL, respectively. The XRD pattern of the L and ZnL exhibited an amorphous character with low crystallinity. The SEM images showed shapeless plates with narrow valleys in the case of L and deep pores in the case of ZnL. The TEM images revealed a cluster of scaffold structures or agglomerated structures of the polymers. The solid-state conductivity of the L and ZnL was studied and the results showed that the conductivity increased by increasing the temperature from 300K to 400K. This behavior confirms the semiconducting properties of L and ZnL. The calculated solid-state conductivity of L in this temperature range (4.18×10^{-10}-1.04×10^{-5} Ω^{-1} m^{-1}) is higher than the calculated solid-state conductivity of ZnL(1.45×10^{-11}-3.12×10^{-9} Ω^{-1} m^{-1}) whereas the calculated activation energy (of conductivity) for ZnL (0.19 ev) is lower than the calculated activation energy of conductivity (0.29ev) for L.*

KEYWORDS: *Ionic Schiff base polymer; Metallopolymer; Semiconducting; Zn^{2+}.*

INTRODUCTION

In recent decades, growing interest has been generated in the field of metallopolymers by many researchers because of their potential application in different areas with special characteristics such as semiconducting and conducting properties, optical, photo-electrical and, redox activity [1-8]. On the other hand, the Schiff base polymers have an important role in the development of this area and have attracted attention due to their properties as well as their biological activities [9- 19]. Therefore, syntheses

**To whom correspondence should be addressed.*

+ E-mail: grivani@du.ac.ir

1021-9986/2023/7/2131-2140 10/$/6.00

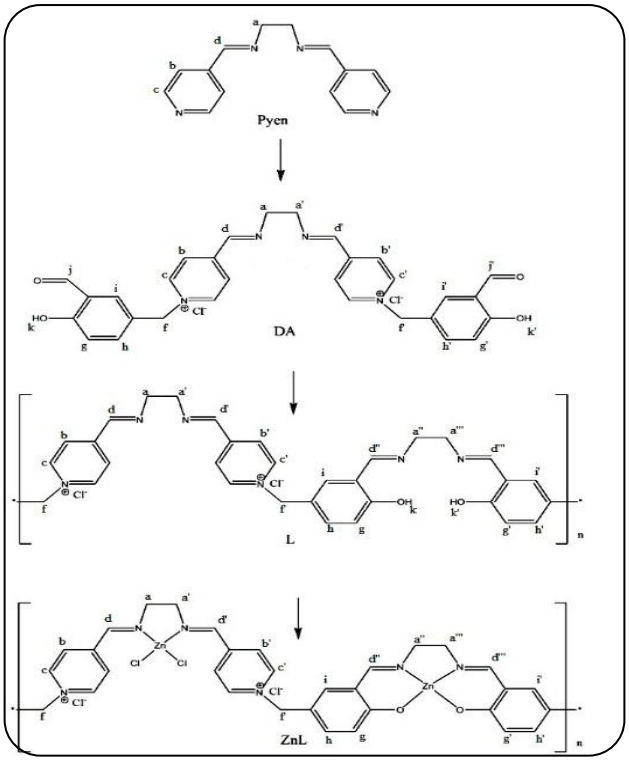

Scheme 1: The synthetic procedures of the polymeric Schiff base ligand and its metallo-Schiff base copolymer

of novel-derived metallopolymers are very important in developing technological applications. The Metallo Schiff base polymers can be prepared by polycondensation of a dialdehyde and a diamine and subsequent metalation of polymeric Schiff base ligand. Thus, the design of new monomeric and/or polymeric Schiff base ligands with special and different characteristics and metalation opens new horizons in materials architecture [20-41]. Recently we introduced to design of new monomeric and polymeric Schiff base ligands containing ionic moieties and the preparation of new metallopolymers. It can be changed each part of these kinds of ligands (aldehyde, diamine, and counter ion) and some new metallopolymers with new different properties can be produced by incorporating metal ions. In this research, it is described the synthesis and characterization of a new ionic Schiff base polymer and its Zn^{2+}-metallopolymer containing pyridinium moiety as an ionic segment (Scheme 1) as well as its solid-state conductivity behavior.

EXPERIMENTAL SECTION

Materials

5-Chloromethyl salicylaldehyde [14] and Pyen were prepared by a method described in the literature [42]. All other reagents and solvents for synthesis and analysis were commercially available purchased from Merck and used without further purifications.

The InfraRed (IR) spectra were recorded on a Perkin Elmer infrared spectrometer model 621 by using KBr pellets. The ^{1}H-NMR spectra were recorded on a JOEL-FX-100 FT NMR instrument in DMSO-D_6 solution and TMS as an internal standard. The elemental analysis of carbon, hydrogen, and nitrogen was carried out on a Perkin-Elmer model-2400 elemental analyzer (CDRI, Lucknow, India). FESEM was analyzed from TESCAN mira3. GPC measurements were performed on a water 150-c GPC system equipped with μ storage, 102-105 Å. The mass spectra of the compounds have been recorded with the Agilent Technology (HP) spectrometer with Pseudo Multiple Reaction Monitoring Mode (PMRM**)**.

Preparation of N, N'-bis-pyridine-4-ylmethylene-1,2-diamine (Pyen)

The Pyen was prepared as described in ref [38]. 4-Pyridine carbaldehyde *(4.82 g, 45.02 mmol)* was added to a solution of ethylenediamine in methanol (*1.35 g*, 22.5 *mmol* in 60 *mL* methanol) in a 100 *mL* round bottom flask and the solution was refluxed for 6 h. After evaporation of solvent under vacuum, the yellow precipitates were recrystallized and dried in air. ^{1}H-NMR (300 MHz, DMSO-D_6)(ppm): *δ 8.75(4H), 8.43(4H), 7.60(2H)* and *3.91(4H).*

Preparation of DA

In a 100 mL round bottom flask containing 60 mL acetonitrile, it was added Pyen (4.00 *g*, 16.80 mmol) and 5- chloromethyl salicylaldehyde (5.73 *g*, 33.60 mmol) and stirred for 16 h. After evaporation of the solvent under vacuum, the blood-red color precipitates were collected and washed three times with tetrahydrofuran and dried in air. ^{1}H-NMR (300 MHz, DMSO-D_6)(ppm): *δ 3.5-4.5(4H), 5.2-6.2(4), 6.5-9.8(14), 10-10.5(2H), 11.4(2H), 13-14.5(2H). Mass: m/z= 579.*

Synthesis of L

In a 100 mL round bottom flask containing 60 mL methanol, it was added DA (3.60 *g*, 6,28 mmol), and ethylenediamine (0.373 *g*, 6.28 mmol) the content was refluxed for 4h with stirring. The solvent was evaporated under a vacuum and the precipitates were washed three

Table 1: The results of the CHN analyses of prepared Pyen and synthesized compounds

Compound	(%)C	(%)H	(%)N
Pyen	70.32 (70.59)*	5.86 (5.88)	22.49 (23.53)
DA	62.04 (62.17)	4.76 (4.83)	9.86 (9.67)
L	63.58 (63.68)	5.28 (5.31)	13.98 (13.93)
Zn P	47.97 (48.06)	3.69 (3.75)	10.58 (10.51)

*Experimental(Theoretical)

Table 2: FT-IR data of Schiff base ligand and polymeric metal complex (ZnL) (cm−1)

Compound	$\upsilon_{C=O}$	$\upsilon_{C=N}$	ν_{M-N}	ν_{M-O}
Pyen	-	1643	-	-
DA	1683	1643	-	-
L	-	1642(for cationic moiety), 1632 (for salycilate moiety)	-	-
Zn L	-	1626,1630	416-620	798-874

times by n-hexane and chloroform and dried in air. ^{1}H-NMR (300 MHz, DMSO-D_6)(ppm): *δ 2.9- 3.2(4H), 3.3-4.5(4H), 5.2-6(4H), 6.5-8.0(6H), 8.2- 9.2(8H), 8.7(2H), 10-10.5(2H), 12-15-(2H). Mass: m/z = 604.*

Synthesis of ZnL

In a 100 mL round bottom flask containing 60 *mL* methanol, it was added L (1 *g*, 1.6 mmol), and $ZnCl_2$ (0.451 *g*, 3.2 mmol), and the content was refluxed for 4 h with stirring. The solvent was evaporated by a rotary evaporator and the solid was washed three times by n-hexane and chloroform and dried in air. ^{1}H-NMR (300 MHz, DMSO-D_6)(ppm): *δ 3-3.2(4H), 4-4.5(4H), 5.5-6.0(4H), 6.5-8.0(6H), 8.9.5(8H), 9.4-10.5(4H). Mass: m/z = 809.*

RESULTS AND DISCUSSION

Elemental analysis and FT-IR spectra

The proposed chemical composition of the regents and polymeric Schiff base ligand and metallo Schiff base polymer was confirmed by elemental (CHN) analysis (Table 1).

FT-IR spectroscopy was also used for the characterization of functional groups in the synthesized polymers. The main variation in the FT-IR spectra in the synthesis of Schiff base compounds is the appearance and disappearance of $\nu_{C=O}$ of the aldehydic band in the formation of DA and L, respectively, and the production of new bands of $\nu_{C=N}$ for the formation of iminic groups. Thus, in the reaction of 5-Chloromethyl salicylaldehyde and Pyen, the new band appeared at 1683 cm^{-1} in the FT-IR spectrum of the DA related to the carbonyl of salicylate moiety. In the synthesis of L, from the reaction of DA and ethylene diamine, in the FT-IR spectrum of L, the original carbonyl band at 1683 cm^{-1} disappeared and a new band at 1632 cm^{-1} appeared, approving the formation of new iminic bands and producing of the polymeric Schiff base ligand of L. The two kinds of iminic bands (for the ethylene diimine of cationic and salicylate moieties) are shifted To the lower wave numbers and appeared at 1626 cm^{-1} and 1630 cm^{-1} by reaction of L and $ZnCl_2$, due to linking of the nitrogen of imines to the Zn^{2+} ions (Table 2).

^{1}H-NMR spectra

The Pyen, DA, L, and ZnL were characterized by ^{1}H-NMR spectroscopy. The ^{1}H-NMR spectra of them are shown in Fig 1, Fig 2, Fig 3, and Fig 4, and all of them were assigned in each spectrum. For the Pyen, there are four kinds of protons that resonated at 3.9, 8.4, 8.7, and 7.6 ppm for the a, b, c, and d proton resonances (Fig. 1). In the case of the DA, it seems that each proton in this compound resonates separately because of torsion of the two imine-pyridinium methylsalycylate moieties about the C─C bond of ethyl group and the spectrum is crowded. The resonances of the ethyl protons (a, a') appeared at the region of 3.5- 4.5 ppm. The methylene protons (f, f') resonate at the region of 5.2- 6.2 ppm. All the aromatic protons (b, b', c, c', i, i', g, g', h, h') exhibit broad-range resonances and appear at regions of 6.5- 9.8 ppm. The broad resonance at the region of 11.4 ppm is attributed to the aldehyde protons (j, j') and the very broad signal at *13.-14.5 ppm* is attributed to the phenolic protons (k, k'). The resonances at *10-10.5 ppm* are ascribed to the iminic

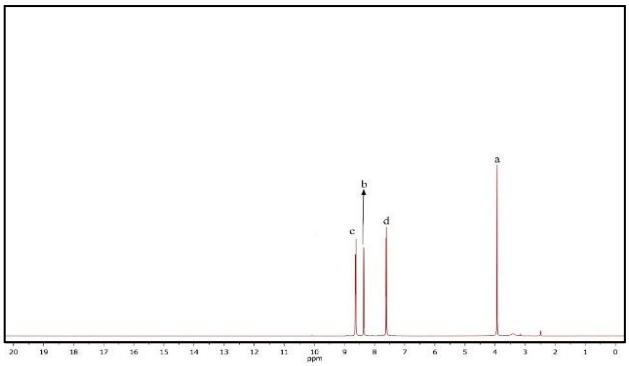

Fig 1: ^{1}H- NMR spectrum (300 MHz) of Pyen in DMSO-d_6 at 298K

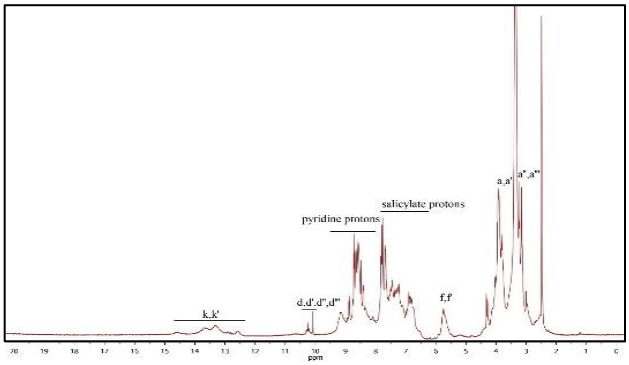

Fig 3: ^{1}H- NMR spectrum (300 MHz) of L in DMSO-d_6 at 298K

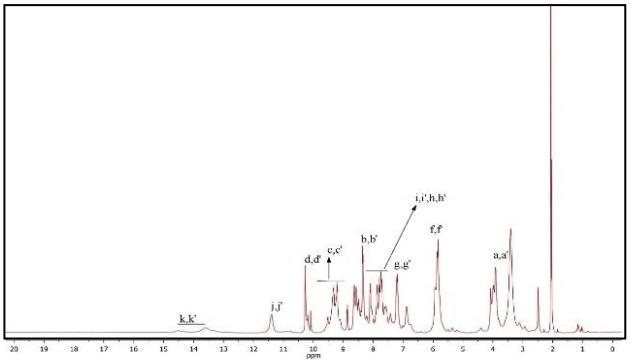

Fig 2: ^{1}H- NMR spectrum (300 MHz) of DA in DMSO-d_6 at 298K

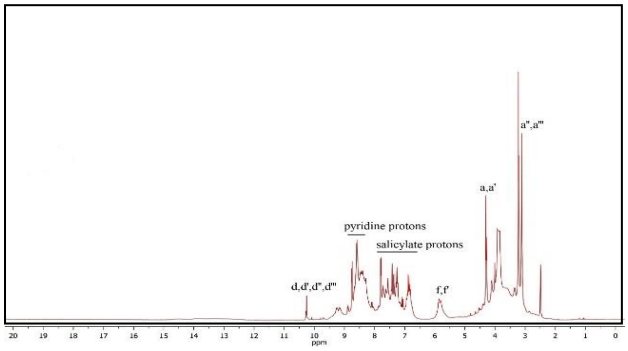

Fig 4: ^{1}H- NMR spectrum (300 MHz) of ZnL in DMSO-d_6 at 298K

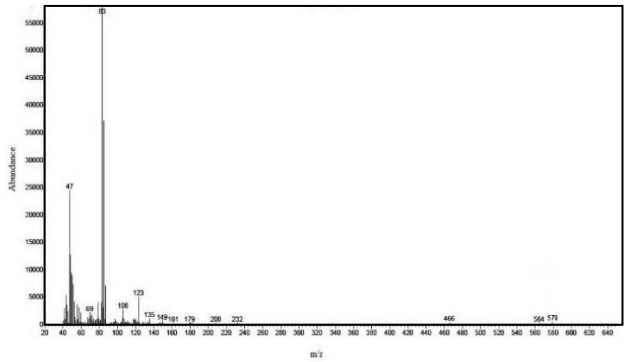

Fig 5: PMRM-- Mass spectrum of DA

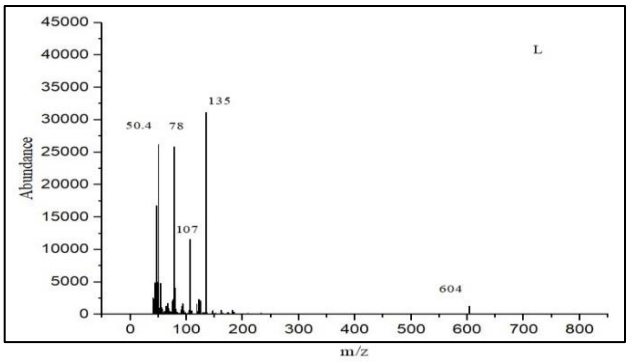

Fig 6: PMRM--Mass spectrum of L

protons of d, d' (Fig 2). In the spectrum of the L, the resonances of aldehydic protons disappeared and some new resonances appeared at the region of 8.78-9 ppm related to the new imine bond formation. The broad bands at the region of 12.2-15.0 ppm are related to the resonances of phenolic protons of salicylate moiety (k, k'). This broadening is attributed to the interaction of nitrogen of iminic bond and OH of salicylate (Fig 3). The spectrum of the ZnL is similar to the spectrum of L alongside to small changes in chemical shifts. In addition, the resonances of the OH protons disappear during the metalation of the L and the formation of ZnL (Fig 4).

Mass spectrometry

The mass spectrometry was used for further characterization of the synthesized compounds. The mass spectral data of synthesized compounds can easily describe the corresponding molecular weights of theme and their fragmentation patterns consistent withe their structures. In many cases, the ionic molecule shows a very low-intensity band and rarely observable. The mass spectrometry analysis of DA, L, and ZnL shows an isotope pattern at m/z = 579, 604, and 809 respectively,

Table 3: The data of size exclusion chromatography of polymers

Polymer	M_n (g/mol)	M_w (g/mol)	PDI	Appearance
L	2609	6141.4	1.56	Yellow
ZnL	3925	14212	1.70	Dark Yellow

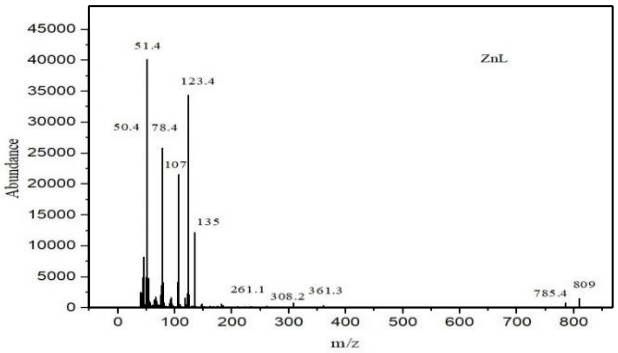

Fig 7: PMRM-Mass spectrum of ZnL

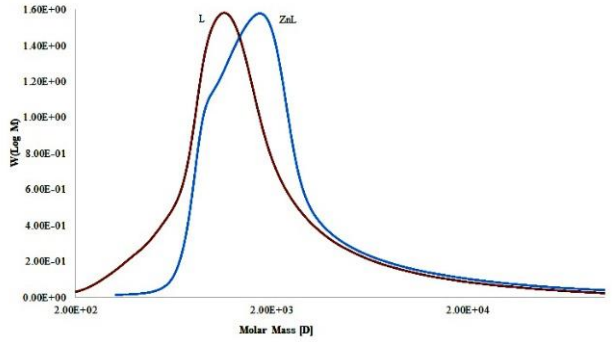

Fig 8: The results of size exclusion chromatography of L and ZnL

corresponding to the molecular weight of DA and the repetitive unit molecular weights of L and ZnL polymers, which is consistent with their predicted molecular weights (Figs. 5, 6, 7). For compounds containing one element with more than one stable and abundant isotope, more than one peak will be observed for every fragment containing that element [42] as it is observed for the bands around the m/z of *47, 69, 83, 123, 135, 149* for the DA and *50.4, 78, 107, 135* for the L and *51.4, 78.4, 107, 123.4, 135* for the ZnL.

Size exclusion Chromatography

The results of molecular weight determination are given in Table 3 and Fig. 8. The molar mass of a polymer was usually expressed as M_n and M_w. From Table 3, these amounts were obtained 2609 g/mol, 6141.4 g/mol for L and 3925 g/mol, 14212 g/mol for ZnL. The polydispersity of these two polymers was given as 1.56 and 1.70, respectively.

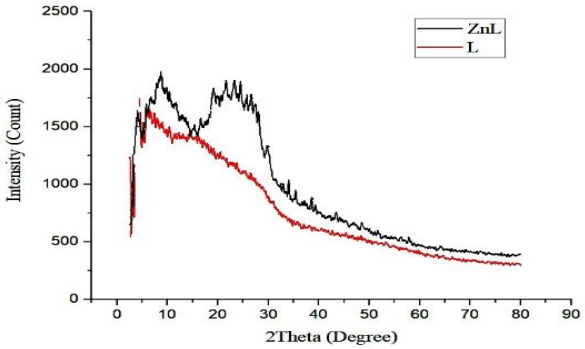

Fig 9: XRD patterns of L and ZnL

Morphological study (XRD, SEM, and TEM)

The XRD patterns of L and ZnL are given in Fig. 9. The two synthesized compounds L and ZnL exhibit broad signals. Thus, these compounds show low crystallinity and it can be stated that they show amorphous property in which the amorphous character of the L is higher than the amorphous character of the ZnL due to exhibiting broad XRD signals of L with respect to ZnL [43].

In order to perform further investigation of the morphological changes of the L and ZnL, SEM technique was used. The SEM images of L and ZnL are presented in Fig. 10. The SEM of the two compounds of L and ZnL shows porous, semi-flat surfaces with shapeless plates. The plates form hollows that in the case of L, they form narrow valleys with high walls whereas in the case of ZnL the shapeless plates adhere together irregularly and produce deep pores. The XRD results of L and ZnL, with some crystallinity for ZnL, consist of the SEM results as it is observed from SEM images of L and ZnL[44-46]. In comparison to other researchers [47-49], the difference in the morphology of the L and ZnL can be related to the coordination of metal ion (Zn^{2+}) to the polymeric ligand of L. This makes the polymer chains that are close to each other easier to fit together and cause pores to surface.

TEM was used for further investigation of the nature and structure of synthesized compounds of L and ZnL (Fig. 11). In two cases, a cluster of scaffold structures is observed, which confirms the polymer generation. The extent of clustering in the case of the ZnL is extremely high due to the formation of coordination bonds and binding of Zn^{2+} to L. The cluster formation or agglomeration, which causes a network with layered morphology, might result from strong electrostatic forces between the polymeric particles because of the ionic character of polymeric chains [50]. Thus, the XRD, SEM, and TEM results are

Table 4: Conductivities and activation energies of conduction for L and ZnL

Material	Conductivity (Ω^{-1} m^{-1})			
	300 K	350 K	400 K	Ea (eV)
L	4.18×10^{-10}	2.11×10^{-7}	1.04×10^{-5}	0.29
Zn L	1.45×10^{-11}	6.08×10^{-10}	3.12×10^{-9}	0.19

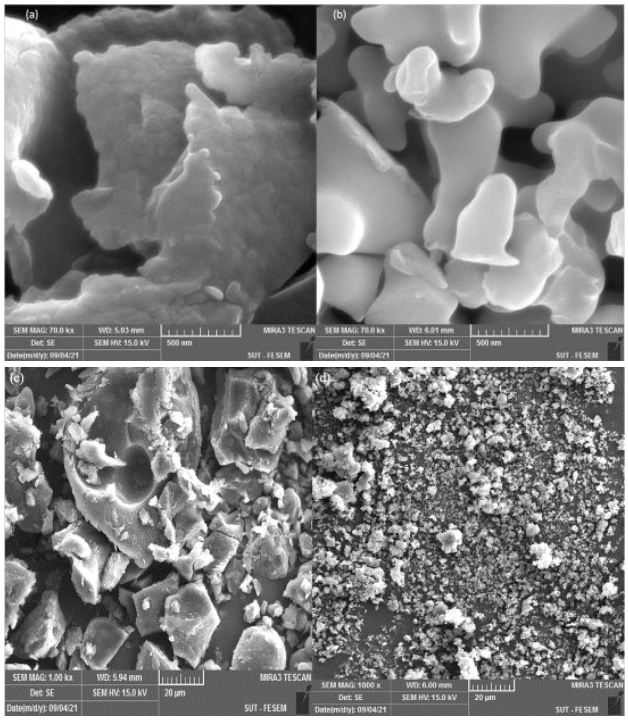

Fig 10: SEM images of (a, b) L and (c, d) ZnL

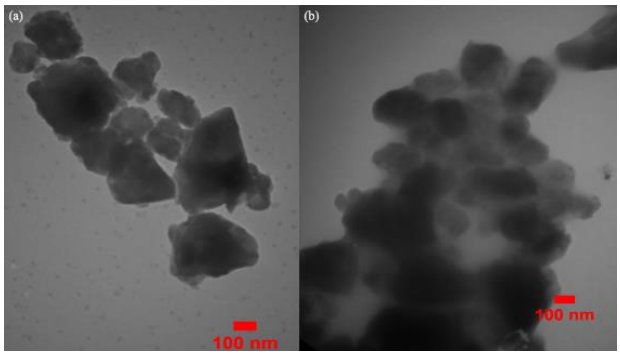

Fig 11: TEM micrographs of (a) L and (b) ZnL.

in agreement together and confirm the amorphous character of L and ZnL with some crystallinity, porosity, and clustering of ZnL.

Solid state conductivity

Recently, great effort is geared toward the investigation of new materials for organic or metal–organic polymers exhibiting solid-state electrical conductivity. In this research, it is elucidated the electrical conductivity of the polymeric ligand of L and its Zn^{2+}-metallopolymer in three temperatures in the range of 300K-400K. The obtained data are given in Table 4.

The general behavior of electrical conductivity is given by the Arrhenius equation (Eq (1)), where E_a is the activation energy for the conduction, σ_0 is a constant for the conductivity independent of temperature, T is the absolute temperature, and k is the Boltzmann constant [51]:

$$\sigma = \sigma_0 \exp(-E_a/kT) \quad (1)$$

The plots of log σ *vs.* 1/T can be informative in the elucidation of electrical conductivity. These plots are given in Fig. 12 for the polymeric ligand(L) and its Zn^{2+} metallopolymer. As observed from this Figure, the solid-state conductivity of the two compounds of L and ZnL increased by increasing the temperature in which the conductivity varied from 4.18×10^{-10} - 1.04×10^{-5} Ω^{-1} m^{-1} and 1.45×10^{-11} - 3.12×10^{-9} Ω^{-1} m^{-1} at the temperature range of 300- 400 K for the L and ZnL, respectively. Thus, these data exhibit that the polymeric ligand (L) and its ionic metallopolymer (ZnL) display moderate semiconducting behavior [52-54]. The electrical conductivity of the ZnL is lower than the L at the investigated temperature range due to the incorporation of Zn^{2+} in polymer chains of L. The calculated activation energy is 0.29 ev for L and 0.19 ev for ZnL. It is observed from the XRD pattern that the amorphous and crystallinity properties were decreased and increased, respectively, by the incorporation of the Zn^{2+} in polymeric chains of L. The binding of Zn^{2+} to the L leads to lowering the flexibility of the chains in the ZnL, reducing the dislocation of chloride ions, which are responsible for the electrical conductivity of these compounds as consistent with the amorphous character of L and ZnL with some crystallinity for ZnL, resulting in the low flexibility of ZnL. This is confirmed by the TEM images in which the clustering and agglomerating were increased by the incorporation of Zn^{2+} into L chains. Because of the presence of two coordination sites in the L, the incorporation of Zn^{2+} increases the folding of chains and this causes the chloride ions to be placed closer together in the chain and reduces the activation energy for the dislocation of chloride ions in ZnL with respect to L. The calculated electrical conductivity of L and ZnL in this research locates about the ranges reported for synthesized Schiff base polymer by *Saçak et al*[57],

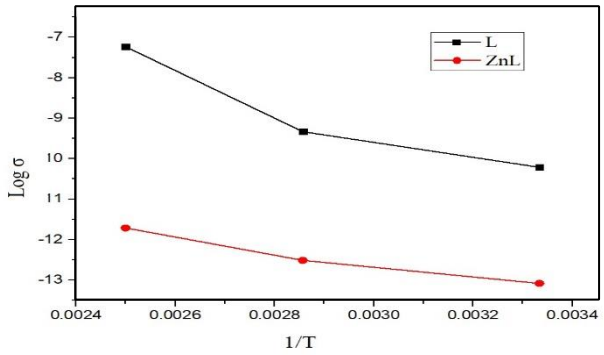

Fig 12: Arrhenius plot of electrical conductivity of L and ZnL

and *Muthusamy et al*[56] and lower than those amounts calculated by *El-Sonbati et al*. [57] and *Higuchi et al.*[58]. Thus, the synthesized compound in this research shows moderate semiconducting properties.

CONCLUSIONS

In conclusion, it was synthesized a new ionic Schiff polymer and its zn^{2+} metallopolymer in simple routes. They were characterized by different methods. CHN analyses confirm the chemical composition of the synthesized polymers. The FT-IR and ^{1}HNMR spectroscopies confirm the functionalities of the polymers and the structures of synthesized polymers. The molecular weights of polymers were determined by size exclusion chromatography. The XRD profiles show the amorphous character of them. The SEM images exhibited the porous and semi-flat surfaces of synthesized polymers. From TEM images it is observed a cluster of scaffold structures confirming the polymer formation of L and ZnL. The conductivity study of the two polymers in the solid-state shows that they have semiconducting behavior in which the conductivity of L is higher than the ZnL but the activation energy of conductivity for ZnL is lower than the activation energy of L.

Acknowledgments

We are grateful to Damghan University (DU) for its financial support.

Received : Sep. 07 , 2022 ; Accepted : Dec. 12, 2022

REFRENCES

[1] Benhaoua C., Ammari A., Bassaid S., Belfedal A., Dehbi A., Physical and Chemical Properties of Dimedone "Base Schiff" for Organic Semiconductor Applications, *J. Electron. Mater.*, **48**: 7792-7798 (2019).

[2] Wang Y. Q., Pan Y., Gao W. Q., Wu Y., Liu C. H., Zhu Y.Y., Construction of Optical Active Metallo-Supramolecular Polymers from Enantiopure Bis-Pybox Ligands, *Tetrahedron*, **75**: 3809-3814 (2019).

[3] Abd-El-Aziz A. S., Abdelghani A. A., Mishra A. K., Optical and Biological Properties of Metal-Containing Macromolecules, *J. Inorg. Organomet. Polym. Mater.*, **30**: 3-41 (2020).

[4] Gao B., Zhang D., Li Y., Synthesis and Photoluminescence Properties of Novel Schiff Base Type Polymer-Rare Earth Complexes Containing Furfural-Based Bidentate Schiff Base Ligands, *Opt. Mater.*, **77**: 77-86 (2018).

[5] Novozhilova M.V., Smirnova E. A., Polozhentseva J. A., Danilova J.A., Chepurnaya I.A., Karushev M.P., Timonov A.M., Multielectron Redox Processes in Polymeric Cobalt Complexes with N_2O_2 Schiff Base Ligands, *Electrochim. Acta*, **282**: 105-115 (2018).

[6] Novozhilova M., Anischenko D., Chepurnaya I., Dmitrieva E., Malev V., Timonov A., Karushev M., Metal-Centered Redox Activity in a Polymeric Cobalt (II) Complex of a Sterically Hindered Salen Type Ligand, *Electrochim. Acta*, **353**: 136496 (2020).

[7] Liu M.J., Wang K., Therapeutic Efficacy Observation on Combining Herbal Cake-Partitioned Moxibustion with Plum-Blossom Needle Therapy for Cervical Radiculopathy, *J. Acupunct. Tuina Sci.*, **11**: 363-366 (2013).

[8] Heeger A. J., Semiconducting Polymers: the Third Generation, *Chem. Soc. Rev.*, **39**: 2354-2371 (2010).

[9] Sun J., Ma Q., Xue D., Shan W., Liu R., Dong B., Shao B., Polymer/inorganic Nanohybrids: An Attractive Materials for Analysis and Sensing, *TrAC, Trends Anal. Chem.*, **140**: 116273 (2021).

[10] Banasz R., Wałęsa-Chorab M., Polymeric Complexes of Transition Metal Ions as Electrochromic Materials: Synthesis and Properties, *Coord. Chem. Rev.*, **389**: 1-18 (2019).

[11] Ho C.L., Wong W.Y., Metal-Containing Polymers: Facile Tuning of Photophysical Traits and Emerging Applications in Organic Electronics and Photonics, *Coord. Chem. Rev.*, **255**: 2469-2502 (2011).

[12] Nozha S. ., Morgan S.M., Ahmed S.A., El-Mogazy M.A., Diab M.A., El-Sonbati A.Z., Abou-Dobara M.I., Polymer Complexes. LXXIV. Synthesis, Characterization and Antimicrobial Activity Studies of Polymer Complexes of some Transition Metals with Bis-Bidentate Schiff Base, *J. Mol. Struct.*, **1227**: 129525 (2021).

[13] Li X., Li J., Kang F., Enhanced Electrochemical Performance of Salen-Type Transition Metal Polymer with Electron-Donating Substituents, *Ionics*, **25**: 1045-1055 (2019).

[14] Khan S. A., Nami S. A., Bhat S. A., Kareem A., Nishat N., Synthesis, Characterization and Antimicrobial Study of Polymeric Transition Metal Complexes of Mn (II), Co (II), Ni (II), Cu (II) and Zn (II) , *Microb. Pathog.*, **110**: 414-425 (2017).

[15] Xie Y., Chen L., Zhang X., Chen S., Zhang M., Zhao W., Zhao C., Integrating Zwitterionic Polymer and Ag Nanoparticles on Polymeric Membrane Surface to Prepare Antifouling and Bactericidal Surface *via* Schiff-Based Layer-By-Layer Assembly, *J. Colloid Interface Sci.*, **510**: 308-317 (2018).

[16] Baran N.Y., Saçak M., Synthesis, Characterization and Molecular Weight Monitoring of a Novel Schiff Base Polymer Containing Phenol Group: Thermal Stability, Conductivity and Antimicrobial Properties, *J. Mol. Struct.*, **1146**: 104-112 (2017).

[17] Barbosa H.F., Attjioui M., Leitão A., Moerschbacher B.M., Cavalheiro É.T., Characterization, Solubility and Biological Activity of Amphihilic Biopolymeric Schiff Bases Synthesized Using Chitosans, *Carbohydr. Polym.*, **220**: 1-11 (2019).

[18] Karimipour G., Rafiee Z., Bahramian M., Peroxynitric Acid: A Convenient Oxygen Source for Oxidation of Organic Compounds Catalyzed by Polyimide-Supported Manganese (III) Tetrakis (4-Methoxylphenyl) Porphyrin Acetate, *Iran. J. Chem. Chem. Eng.*, **36**: 17-28 (2017).

[19] Kaczmarek M. T., Zabiszak M., Nowak M., Jastrzab R., Lanthanides: Schiff Base Complexes, Applications in Cancer Diagnosis, Therapy, and Antibacterial Activity, *Coord. Chem. Rev.*, **370**: 42-54 (2018).

[20] Noroozi M., Ghahri Saremi S., Synthesis of Schiff Base-functionalized Fullerene Anchored Palladium Complex as a Recyclable Nanocatalyst in the Heck Reaction and Oxidation of Alcohols, *Iran. J. Chem. Chem. Eng. (IJCCE)*, **40(5)**: 1395-1405 (2021).

[21] Nguyen M.T., Jones R.A., Holliday B.J., Recent Advances in the Functional Applications of Conducting Metallopolymers, *Coord. Chem. Rev.*, **377**: 237-258 (2018).

[22] Gohy J.F., Lohmeijer B.G., Schubert U.S., Metallo Supramolecular Block Copolymer Micelles, *Macromolecules.*, **35**: 4560-4563 (2002).

[23] Xu L., Ho C.L., Liu L., Wong W.Y., Molecular/ Polymeric Metallaynes and Related Molecules: Solar Cell Materials and Devices, *Coord. Chem. Rev.*, **373**: 233-257 (2018).

[24] Mauro M., Bellemin-Laponnaz S., Cebrián C., Metal-Containing Polymers as Light-Emitting and Light-Responsive Materials and Beyond, *Chem. Eur. J.*, **23**: 17626-17636 (2017).

[25] Atar A.B., Jeong J.Y., Kim N., Park J.S., Metallo-Supramolecular Polymers Made of Cobalt and 3, 4-Propylenedioxythiophene-Bisterpyridine Complexes for Electrochromic Applications, *Macromol. Res.*, **26**: 814-818 (2018).

[26] Liu Q., Guo Y., Wu T., Chen M., Xie T., Wang P., Novel Terpyridine-bridged Parallel Dication Metallo-Bisviologens and Their Supramolecular Complexes, *Chem. Res. Chin. Univ.*, **35**: 229-234 (2019).

[27] Hassan M., Hassan E., Fadel S.M., Abou-Zeid R.E., Berglund L., Oksman K., Metallo-Terpyridine-Modified Cellulose Nanofiber Membranes for Papermaking Wastewater Purification, *J. Inorg. Organomet. Polym. Mater.*, **28**: 439-447 (2018).

[28] Zou F., Chen H., Chen S., Zhuo H., Development of Supramolecular Shape-Memory Polyurethanes Based on Cu (II)–Pyridine Coordination Interactions, *J. Mater. Sci.*, **54**: 5136-5148 (2019).

[29] Zhang K.Y., Liu S., Zhao Q., Huang W., Stimuli–Responsive Metallopolymers, *Coord. Chem. Rev.*, **319**: 180-195 (2016).

[30] Mondal S., Yoshida T., Rana U., Bera M. K., Higuchi M., Thermally Stable Electrochromic Devices Using Fe (II)-Based Metallo-Supramolecular Polymer, *Sol. Energy Mater. Sol. Cells*, **200**: 110000 (2019).

[31] El-Bindary A.A., El-Sonbati A.Z., Diab M.A., Ghoneim M.M., Serag L.S., Polymeric Complexes—LXII. Coordination Chemistry of Supramolecular Schiff Base Polymer Complexes—A review, *J. Mol. Liq.*, **216**: 318-329 (2016).

[32] Motakef-Kazemi N., Asadi A., Methylene Blue Adsorption from Aqueous Solution Using Zn_2 (BDC)2 (DABCO) Metal Organic Framework and Its Polyurethane Nanocomposite, *Iran. J. Chem. Chem. Eng. (IJCCE)*, **41(12):** 4026-4038 (2022).

[33] Ranjbar M., Mirzaei S., Moshafi M. H., Bahadori A., Evaluation, Preparation and Characterization of Chitosan/ZnO Nanocomposite and Antibacterial Activity Against Pathogenic Microbial Strains, *Iran. J. Chem. Chem. Eng. (IJCCE),* **41(4):** 1119-1125 (2022).

[34] Amangah M., Salami Kalajahi M., Roghani-Mamaqani H., Effect of 1, 2, 3-Trichloropropane as tri-Functional Monomer on Thermophysical Properties of Poly (Ethylene Tetrasulfide), *Iran. J. Chem. Chem. Eng. (IJCCE),* **39(2):** 243-249 (2020).

[35] Zhou X.F., Fast Pyrolysis of Napier Grass Catalyzed by Encapsulated Cu ([H4] Salen), *Iran. J. Chem. Chem. Eng. (IJCCE),* **39(4):** 243-249: 91-98 (2020).

[36] Bai L., Tao F., Li L., Deng A., Yan C., Li G., Wang L., A Simple Turn-On Fluorescent Chemosensor Based on Schiff Base-Terminated Water-Soluble Polymer for Selective Detection of Al^{3+} in 100% Aqueous Solution, *Spectrochim. Acta, Part A*, **214**: 436-444 (2019).

[37] Xie M., Tang J., Fang G., Zhang M., Kong L., Zhu F., Zhan J., Biomass Schiff Base Polymer-Derived N-Doped Porous Carbon Embedded with CoO Nanodots for Adsorption and Catalytic Degradation of Chlorophenol by Peroxymonosulfate, *J. Hazard. Mater.*, **384**: 121345 (2020).

[38] Betiha M.A., El-Henawy S.B., Al-Sabagh A.M., Negm N. A., Mahmoud T., Experimental Evaluation of Cationic-Schiff Base Surfactants Based on 5-Chloromethyl Salicylaldehyde for Improving Crude Oil Recovery and Bactericide, *J. Mol. Liq.*, **316**: 113862 (2020).

[39] Gupta K.C., Abdulkadir H.K., Chand S., Polymer-Immobilized N, N′-Bis (Acetylacetone) Ethylenediamine Cobalt (II) Schiff Base Complex and its Catalytic Activity in Comparison with that of its Homogenized Analogue, *J. Appl. Polym. Sci.*, **90**: 1398-1411 (2003).

[40] Dehno Khalaji A., Ghorbani M., Dusek M., Eigner V., Nickel (II) and Copper (II) Complexes of a New Tetradentate Schiff Base Ligand: Synthesis, Characterization, Thermal Studies and Use as Precursors for Preparation of NiO and CuO Nanoparticles, *Iran. J. Chem. Chem. Eng. (IJCCE),* **37(6):** 27-34 (2018).

[41] Dehno Khalaji A., Shahsavani E., Dusek M., Kucerakova M., Eigner V., Synthesis, Characterization, and Crystal Structures of a Thiosemicarbazone Ligand and its Silver(I) Complex, *Iran. J. Chem. Chem. Eng. (IJCCE),* **39(4):** 23-28 (2020).

[42] Tang Z., Chen X., Pang X., Yang Y., Zhang X., Jing X., Stereoselective Polymerization of Rac-Lactide Using a Monoethylaluminum Schiff Base Complex, *Biomacromolecules*, **5**:65-970 (2004).

[43] Nunn I., Eisen B., Benedix R., Kisch H., Control of Electrical Conductivity by Supramolecular Charge-Transfer Interactions in (Dithiolene) Metalate-Viologen Ion Pairs, *Inorg. Chem.*, **33**: 5079-5085 (1994).

[44] Karamian E., Abdellahi M., Khandan A., Abdellah S., Introducing the Fluorine Doped Natural Hydroxyapatite-Titania Nanobiocomposite Ceramic, *J. Alloys. Compd*, **679**: 375-383 (2016).

[45] Sahmani S., Saber Samandari S., Khandan A., Aghdam M.M., Nonlinear Resonance Investigation of Nanoclay Based Bio-Nanocomposite Scaffolds with Enhanced Properties for Bone Substitute Applications, *J. Alloys. Compd*, **773**: 636-653 (2019).

[46] Wanjari N., Chaudhary Bagade R.G., M.B., Paliwal L.J., Transition Metal Coordination Polymers: Microwave-assisted Synthesis, Morphology, Conductivity, and Decomposition Kinetics by TG/DTA Techniques, *J. Chin. Adv. Mater. Soc.*, **6**: 234-254 (2018).

[47] Abdellahi M., Najfinezhad, A., Saber-Samanadari S., Khandan A., Ghayour H., Zn and Zr Co-Doped M-Type Strontium Hexaferrite: Synthesis, Characterization and Hyperthermia Application, *Chin. J. Phys.*, **56**: 331-339 (2018).

[48] Ghayour H., Abdellahi M., Ozada, N., Jabbrzare S., Khandan A., Hyperthermia Application of Zinc Doped Nickel Ferrite Nanoparticles, *J. Phys. Chem. Solids.*, **111**: 464-472 (2017).

[49] Ghayour H., Abdellahi M., Nejad M. G., Khandan A., Saber-Samandari S., Study of the Effect of the Zn^{2+} Content on the Anisotropy and Specific Absorption Rate of the Cobalt Ferrite: the Application of Co_{1-x} Zn_x Fe_2O_4 Ferrite for Magnetic Hyperthermia, *J. Aust. Ceram. Soc.*, **54**: 223-230 (2018).

[50] Zafar F., Azam M., Sharmin E., Zafar H., Haq Q.M. R., Nishat N., Nanostructured Coordination Complexes/Polymers Derived from Cardanol: "One-Pot, Two-Step" Solventless Synthesis and Characterization, *RSC adv.*, **6**: 6607-6622 (2016).

[51] Elshafaie A., Abdel-Rahman L.H., Abu-Dief A.M., Hamdan S.K., Ahmed A.M., Ibrahim E.M.M., Electric, Thermoelectric and Magnetic Properties of Nickel (II) Imine Nanocomplexes, *Nano*, **13**: 1850074 (2018).

[52] Ibrahim E.M.M., Abdel-Rahman L.H., Abu-Dief A.M., Elshafaie A., Hamdan S.K., Ahmed A.M., The Electric and Thermoelectric Properties of Cu (II)-Schiff Base Nano-Complexes, *Phys. Sci.*, **93**: 055801 (2018).

[53] Abdel Rahman L.H., Abu-Dief A.M., El-Khatib R.M., Abdel-Fatah S.M., Adam A.M., Ibrahim E.M.M., Sonochemical Synthesis, Structural Inspection and Semiconductor Behavior of Three New Nano Sized Cu (II), Co (II) and Ni (II) Chelates Based on Tri-dentate NOO Imine Ligand as Precursors for Metal Oxides, *Appl. Organomet. Chem.*, **32**: e4174 (2018).

[54] Ibrahim E.M.M., Abdel-Rahman L.H., Abu-Dief A.M., Elshafaie A., Hamdan S. K., Ahmed A.M., The synthesis of CuO and NiO Nanoparticles by Facile Thermal Decomposition of Metal-Schiff Base Complexes and an Examination of Their Electric, Thermoelectric and Magnetic Properties, *Mater. Res. Bull.*, **107**: 492-497 (2018).

[55] Baran N.Y., Saçak M., Preparation of Highly Thermally Stable and Conductive Schiff Base Polymer: Molecular Weight Monitoring and Investigation of Antimicrobial Properties, *J. Mol. Struct.*, **1163**: 22-32 (2018).

[56] Dineshkumar S., Muthusamy A., Synthesis and Spectral Characterization of Cross Linked Rigid Structured Schiff Base Polymers: Effect of Substituent Position Changes on Optical, Electrical and Thermal Properties, *Polym. Plast. Technol. Eng.*, **55**: 368-378 (2016).

[57] Diabb M.A., El-Sonbati A.Z., Salem O.L., El-Ghamaz N.A., D.C. Electrical Conductivity and Conduction Mechanism of Some Azo Sulfonyl Quinoline Ligands and Uranyl Complexes, *Spectrochim Acta A.*, **83**: 61-66 (2011).

[58] Pandey R.K., Delwar Hossain M.D., Moriyama S., Higuchi M., ionic Conductivity of Ni (II)-Based Metallo-Supramolecular Polymers: Effects of Ligand Modification, *J. Mat. Chem A.*, **1**: 9016-9018 (2013).